Applied Catalysis B: Environmental 245 (2019) 635–647

Contents lists available at ScienceDirect

Applied Catalysis B: Environmental

journal homepage: www.elsevier.com/locate/apcatb

Facile control of defect site density and particle size of UiO-66 for enhanced hydrolysis rates: insights into feasibility of Zr(IV)-based metal-organic framework (MOF) catalysts

Kie Yong Cho[a,b,1], Jin Young Seo[a,1], Hyun-Ji Kim[a], Sung Jin Pai[c], Xuan Huy Do[a,d], Ho Gyu Yoon[e], Seung Sang Hwang[a], Sang Soo Han[c], Kyung-Youl Baek[a,d,f,*]

[a] Materials Architecturing Research Center, Korea Institute of Science and Technology, Seoul 02792, Republic of Korea
[b] Artie McFerrin Department of Chemical Engineering, Texas A&M University, College Station, TX, 77843-3122, United States
[c] Computational Science Research Center, Korea Institute of Science and Technology, Seoul 02792, Republic of Korea
[d] Division of Nano & Information Technology, KIST School, Korea University of Science and Technology, Seoul 02792, Republic of Korea
[e] Department of Materials Science and Engineering, Korea University, Seoul 02841, Republic of Korea
[f] Center for Convergent Chemical Process, Korea Research Institute of Chemical Technology, 141, Gajeong-Ro, Yuseong-Gu, Daejeon 34114, Republic of Korea

ARTICLE INFO

Keywords:
UiO-66
Metal-organic frameworks
Polyethyleneimines
Modulation of MOFs
Lewis acid catalyzed hydrolysis reactions
Chemical warfare agents

ABSTRACT

A catalytic hydrolysis rate of nerve agents can be a significant issue because of their severe toxicity which can lead to severe damage to human life. Regarding the issue, much effort has been given rise to the development of the various design of Zr(IV)-based MOF catalysts so that high catalytic performance. However, we still have feasibility issues. To this end, we turned our attention to develop the method for facile, scalable, and efficient synthesis of Zr(IV)-based MOFs (UiO-66) with high-performance hydrolysis by imparting enriched active sites to the catalysts, as well as to examine its feasibility using the combination of UiO-66 with the organic bases including 4-ethylmorpholine (4-EM) and linear-/ branch-type polyethyleneimine (PEI). The modulated UiO-66 catalysts were synthesized by varying the total reaction concentration. The synthesized three different UiO-66 catalysts were characterized and then applied for hydrolysis rates of the methylparaoxon (MPO) nerve agent simulant. From these investigations, we found that the highest concentration led to the smallest particle size (ca. 100 nm) and highest defect density (1.8 per cluster), resulting in 3-times higher catalytic activity ($0.548\ s^{-1}$) in turnover frequency (TOF) relative to that of the uncontrolled UiO-66 (ca. 580 nm and 1.6 per cluster) ($0.188\ s^{-1}$) which is prepared by the reported procedure. In addition, the reaction process significantly influenced on the catalytic activity of UiO-66, in which the simple change of the reagent mixing method led to a ca. 182-times difference in the catalytic activity for MPO hydrolysis despite using the same reagents including catalysts and bases. Importantly, we found that the reaction process-dependent catalytic activity of UiO-66 can be significantly associated with the chelation of Zr(IV) Lewis acidic active sites by base materials of 4-EM and PEI (Lewis base). Furthermore, the solid-state catalytic system based on the polymer composite of UiO-66S/LPEI10k on the cotton fabric was also examined for MPO hydrolysis at various relative humidity and temperature conditions to create actual atmosphere conditions, which gave the possibility for actual military applications such as protective suits and equipment. In addition, we schematically demonstrated the loss of active sites on UiO-66 by chelation effects based on experimental and density functional theory (DFT)-derived computational simulation because it is highly correlated to the feasibility of Zr(IV)-based MOF catalysts for detoxification of nerve agents. In addition, we carefully propose a plausible reaction mechanism step on the nucleophilic attack by hydroxide group on the basis of the computational simulation.

1. Introduction

Metal-organic frameworks (MOFs) with distinctive features, including various framework structures, porous crystalline systems, large surface area, and a simple modification of metal ions and bridging ligands, have generated intriguing attention for applications in the gas

* Corresponding author at: Materials Architecturing Research Center, Korea Institute of Science and Technology, Seoul 02792, Republic of Korea.
E-mail address: baek@kist.re.kr (K.-Y. Baek).
[1] These authors contributed equally.

https://doi.org/10.1016/j.apcatb.2019.01.033
Received 29 July 2018; Received in revised form 29 December 2018; Accepted 12 January 2019
Available online 14 January 2019
0926-3373/

capture/ storage/ separation, molecular sensing, heterogeneous catalysis, and drug delivery [1–3]. Notably, the accessible and unsaturated metal sites in the frameworks can provide site-isolated catalytically active centers, which have made MOFs rise to a potentially crucial material in the catalysis approaches [4–6]. Within the tremendous family of MOFs, UiO-66 (UiO = University of Oslo), comprising Zr(IV)-carboxylate clusters ($Zr_6(\mu_3\text{-}O)_4(\mu_3-OH)_4(C_8H_4O_4)_6$) ligated by 12 bidentate 1,4-benzenedicarboxylate (BDC) linkers, has been extensively investigated for its catalytic activity based on its significantly robust thermal and chemical stability [7–10].

UiO-66 has shown significant achievements in the promoted hydrolysis of organophosphate nerve agents (Sarin, VS, GD, and Soman) and their simulants [11]. Although the use of UiO-66 in the previous reports have exhibited remarkable catalytic activities in hydrolyzing a methylparaoxon (MPO) nerve agent simulant by the presence of a 4-EM base, exhibiting 19–50 min half-life ($t_{1/2}$), it has insufficient feasibility for an application of real-time decontamination [11,12]. Hence, the enhanced hydrolysis rate in the detoxification applications has been continuously desired for a saving human life along with the environmental purification systems. Many researchers have contributed to investigating Zr-based MOFs with functionalization strategies for by the introduction of functional groups including nitryl (NO_2), hydroxyl (OH), amino (NH_2), and dimethylamino (NMe_2) particularly at the 2- or/and 5- position of BDC [13,14]. Specifically, the presence of the amino groups into UiO-66 (UiO-66-NH_2) exhibited 35-fold enhanced the catalytic activity (turnover frequency, TOF: 0.15 s^{-1}) for hydrolyzing MPO relative to UiO-66 (TOF: 0.004 s^{-1}) because the introduced amino groups played as a Brønsted base, which can promote the hydrolysis of MPO [13,15]. However, the ligand functionalization approaches commonly required difficult and expensive chemical reaction steps.

Another recent approach was the synthesis of UiO-66 analog using Ce (IV) instead of Zr(IV) in the frameworks because of its superior activity than that of Zr(IV) in homogeneous conditions [16]. The hydrolysis rate for MPO was indeed reduced, exhibiting from 19 (UiO-66-Zr) to 8 min (UiO-66-Ce) in $t_{1/2}$, albeit the average particle size of UiO-66-Ce was almost twice larger than that of UiO-66. Although the use of more active metal ions instead of Zr(IV) showed a better hydrolysis rate, the approach using Ce (IV) into UiO-66 can be limited in the specific case of MOFs because Lewis acid metal ions with different acidities can be undertaken by following different framework mechanisms [17–20]. In addition, only few metal ions in the homogeneous system showed high hydrolysis rate for organophosphate ester groups, such as the order sequentially followed by Ce(IV) ≫ Zr(IV) > Hf(IV)˜ Pd(II)˜ Yb(III). This indicates that enhanced hydrolysis by alteration of metal ions from Zr(IV) can be restricted [21–23].

The approaches for the modulation of MOFs have been considered significantly intriguing strategies to provide highly enhanced catalytic activities to Zr(IV)-based MOFs [24–26]. Vermoortele *et al.* suggested that thermal activation of UiO-66 can afford a large number of open sites of Zr(IV) by dehydroxylation of the hexanuclear Zr clusters and a post-synthetic removal of terminated modulators from Zr(IV) nodes [26]. This simple modification of UiO-66 for increased Zr(IV) open sites in UiO-66 led to substantially enhanced catalytic activity in Lewis acidic sites catalyzed reactions. On the basis of the known hydrolysis mechanism of MPO under the presence of Zr(IV)-based MOFs, the open and water (H_2O) coordinated Zr(IV) sites worked as highly active sites relative to the hydroxylated Zr(IV) [27]. In the recent report from Farha's group, the reaction with Nu-1000, which is a Zr(IV)-based MOF, was promoted once forming the ligation between Zr(IV) and MPO by substitution with H_2O ($+21.8\ kJ\ mol^{-1}$) because the catalytic activation energy for its hydrolysis is dramatically downhill by $-48\ kJ\ mol^{-1}$ [28,29]. In addition, the dehydrated Zr(IV) sites can more easily bind with MPO in comparison to H_2O coordinated sites, exhibiting the 10-times faster hydrolysis rate for MPO than that of UIO-66 and NU-1000 without dehydration treatment [28,29]. To that end, we focused on the control of the active sites during the synthesis of MOF by adjusting a number of missing linkers on UiO-66. Furthermore, we also consider the particle size of UiO-66 for a high catalytic hydrolysis rate by providing the large surface area in the interface [30].

In the insight into the feasibility, the linear polyethyleneimine (LPEI) solid-state base has been examined instead of the liquid-state and volatile 4-EM [16,31]. This approach was importantly based on the low solubility of LPEI in water in addition to coating or/and composite techniques for potential applications. However, the performance of LPEI in the hydrolysis of MPO was examined using the as-prepared suspension of LPEI and MOFs in water albeit the common applications required the long retention time for the actual applications. From this approach, we have considered that unsaturated active sites (unsaturated Lewisacidic sites) in the MOF catalysts can be tolerated without both chelating and substitution of H_2O by abundant Lewis base sites in PEI in the composite or/and solution states, which are desired for their uniform and high-quality introduction into suggested applications. This issue should be addressed toward going closer to the actual demands with the PEI candidates.

Herein, we synthesized the water-stable UiO-66 with controlled methods particularly in the density of unsaturated Lewis acidic sites and particle size with the enhanced catalytic hydrolysis rate of MPO. The controlled UiO-66 catalysts were examined for hydrolysis of MPO under the presence of 4-EM, exhibiting that the UiO-66 with the smallest size (ca. 100 nm) along with a more significant number of missing linkers (1.8) (UiO-66S) led to the best performance. The acquired UiO-66S was used for optimization of reaction processes. The different reaction process, particularly in the UiO-66 addition step to the reaction solution, led to the significant changes in the hydrolysis rate of MPO. Among the introduced reaction process, the method, which is an addition of UiO-66 to the MPO/4-EM mixture solution, exhibited the 110-fold higher TOF value relative to the result by the method which is the addition of MPO to the UiO-66/4-EM mixture solution. For the feasibility of UiO-66, we also examined the branch- (BPEI) and linear- (LPEI) type of PEI polymer bases in the hydrolysis of MPO in the aqueous solution state. In particular, the combination of UiO-66 and LPEI was prepared as a polymer composite and applied for the coating system on the cotton fabric supporter to consider the possibility of actual military protective suits and equipment. The polymer composite of UiO-66/LPEI on the cotton fabric was then examined for MPO hydrolysis at the various relative humidity and temperature conditions to create actual atmospheric conditions. The quantum chemical calculations based on density functional theories (DFT) calculation were performed for better clarity to evidence the MPO hydrolysis rate alterations and its reaction mechanism. On the basis of the schematically designed experimental and DFT-based computational investigations, we demonstrated that the Lewis acidic sites of Zr(IV) are not catalytically stable and may not be preserved well because of strong reactivity with Lewis basic sites of the applied base materials. Furthermore, the quantum chemical calculations of the MPO hydrolysis newly suggested an unsolved reaction mechanism step of nucleophilic attack by the hydroxide group to lead the dissociation of the leaving group in the MPO structure.

2. Experimental section

2.1. Materials

The reagents, including zirconium(IV) chloride (ZrCl4, ≥ 99.5%), hydrochloric acid (HCl, 36.5˜38.0%), benzene-1,4-dicarboxylic acid (BDC, 98%), dimethylformamide (DMF, 99.8%), 4-ethylmorpholine (4-EM, 97%), linear type polyethyleneimine (LPEI, M_n = 10k), and branch type polyethyleneimine (BPEI, M_n = 0.6k and 10k) were purchased from Sigma-Aldrich and were used as received unless otherwise noted. Methylparaoxon (MPO, Sigma-Aldrich) was used after dilution in methanol (0.253 mmol mL^{-1}).

2.2. Synthesis of UiO-66 catalysts with a different size and its scale-up procedure

The modulated UiO-66 catalysts were synthesized by modifying the reported protocols [8,32,33]. We prepared the two separated solutions that one contained $ZrCl_4$ (1.62 mmol, 0.38 g), one-third of the DMF, and HCl (1.5 mL) and another one included BDC (2.25 mmol, 0.37 g) and the remained DMF and then stirred at 50 °C until well dissolved. The total DMF volume was changed for modulation of UiO-66, specifically used 45 mL for UiO-66L (large size), 22.5 mL for UiO-66M (medium size), and 11.25 mL for UiO-66S (small size). The reaction was allowed by pouring the above solution into the latter solution and heating at 80 °C and thereafter retained for 24 h. After dilution with DMF of the same volume used for the reaction, the precipitates were filtered and then washed with an excess of DMF and ethanol continuously. The acquired UiO-66 were dried at 90 °C for overnight and then activated by drying at 150 °C for 3 h before applying as a catalyst. The scale-up procedure for UiO-66S was undertaken with 200-times larger scale, and the procedures were the same as described for the synthesis of UiO-66S.

2.3. Evaluation for hydrolysis of MPO in an aqueous solution system

The hydrolysis reaction of MPO catalyzed by UiO-66 was monitored by ^{31}P NMR. **(1) *Method 1*:** The 5 mL vial with a 0.58 mL H_2O/D_2O (9/1) mixture was prepared and sequentially added 4-EM (0.45 mmol) and 0.1 mL of diluted MPO in methanol (0.253 mmol mL^{-1}). After stirring for 30 s, 0.32 mL of UiO-66 suspension in water was finally added in a minute to the formerly prepared solution. After a predetermined time, 20 μL of sample was taken and then diluted with 0.7 mL of D_2O. Thereafter, the diluted solution was filtered to remove the UiO-66 catalysts. The acquired solution was used for evaluation of the hydrolysis rate by ^{31}P NMR. **(2) *Method 2:*** The 5 mL vial with a 0.58 mL H_2O/D_2O (9/1) mixture was prepared and sequentially added 4-EM (0.45 mmol) and 0.32 mL of UiO-66 suspension in water (5 mg mL^{-1}). After stirring for a day, 0.1 mL of diluted MPO in methanol (0.253 mmol mL^{-1}) was finally added to the formerly prepared solution. Evaluation of the hydrolysis rate was performed by following the procedure used in ***Method 1***. (3) ***Method 3*:** The 5 mL vial with a 0.58 mL H_2O/D_2O (9/1) mixture was prepared and sequentially added 4-EM (0.45 mmol) and 0.32 mL of UiO-66 suspension in water (5 mg mL^{-1}). After stirring for 30 s, 0.1 mL of diluted MPO in methanol (0.253 mmol mL^{-1}) was finally added in a minute to the formerly prepared solution. In the case of the reactions with BPEI, we performed the in-situ reaction method, in which the prepared reaction solution according to ***Method 1*** or ***Method 2*** was then transferred to the NMR tube, and the ^{31}P NMR spectra were immediately measured without further sampling.

2.4. Evaluation for hydrolysis of MPO in the polymer composite system at various relative humidity and temperature conditions

The UiO-66/LPEI composite catalysts coated on the cotton fabric supporter were applied for MPO hydrolysis under control of the relative humidity and temperature. 4.5 mg of LPEI10k was first dissolved in 0.2 mL of methanol. The UiO-66S catalyst was dispersed in 0.2 mL of the LPEI10k solution (22.5 mg mL^{-1}) via sonication. The cotton fabric was coated by simple drop casting of the UiO-66S/LPEI10k suspension. The UiO-66S/LPEI10k composite catalysts were then dried under vacuum for 24 h to remove residue methanol. The 20 μL of the MPO solution (1.0 mmol mL^{-1} in methanol) was dropwise onto the UiO-66/LPEI10k coating surface on the cotton fabric. Thereafter, the UiO-66/LPEI10k-coated composite catalysts were transferred to the temperature and humidity control chamber (P-TH31, Labmate, South Korea). After the predetermined time, the UiO-66/LPEI10k composite cotton fabric was extracted using methanol-d_4 for washing out the residual MPO and its hydrolyzed resultants (*p*-nitrophenol and dimethoxy phosphate). The extracted solution was used to determine the reaction conversion by ^{31}P NMR.

2.5. Computational details

To investigate chemical reactions between UiO-66 structures and small agents, density functional theory (DFT) calculations were carried out within the framework of M06-L Meta-Generalized Gradient Approximation [34]. Here, for non-metal atoms, the def2-SVP basis set was used, and, for Zr, SRSC pseudo-potential was considered to effectively describe the outer valence region [35,36]. All total energies for optimized structures were corrected by considering the zero-point energy, and free energy change for the chemical reactions between UiO-66 and agents was computed at 298 K, which was obtained through frequency calculations. The DFT calculations were performed with Q-Chem 5.0 modeling suit [37]. To represent UiO-66MOF structure, we used a cluster model such as: the local framework of UiO-66 consists of six Zr atoms, eight oxygen atoms, and twelve bridging ligands, so the total number of atoms for the unit structure of UiO-66 is 186 ea. This number is too large to calculate for the present calculation level that the benzene rings of the twelve ligands be omitted to focus on the interaction on the metal sites and terminated with hydrogen atoms. For defect description, one carboxylate ligand (COOH) is omitted, and two Zr atoms are exposed to water molecule or agents. One Zr site is assumed to be occupied by hydroxyl group for all geometries, which is reasonable due to its high binding energy as will be shown later.

2.6. Characterizations

Powder X-ray diffraction (PXRD) patterns were acquired on a Rigaku diffractometer (Rigaku Smart Lab, Rigaku Co., Japan) operated at 45 kV and 40 mA with CuKα radiation (λ = 1.5406 A°) using a diffracted beam monochromator. Data were collected between 2θ = 5° and 35° at 0.01° intervals. X-ray photoelectron spectroscopy (XPS) analysis was performed under reduced pressure using an X-ray photoelectron spectrometer (X-TOOL, ULVAC-PHI) with a monochromatic AlKα source. Potentiometric titrations were performed with a Titrando 905 (Metrohm) equipped with Dosino 800 (Metrohm). Thermal analysis was performed by thermogravimetric analysis (TGA, TA instruments TGA 2950) at a heating rate of 10 °C min^{-1} under N_2. ^{1}H NMR and ^{31}P NMR spectra were recorded in H_2O/D_2O = 9/1 (v/v) at 25 °C on a Varian Unity INOVA (300 MHz). Fourier transform infrared (FT-IR) spectra were measured by Thermo Scientific Nicolet FT-IR system (iS10) using a solvent casting method on KBr pellets. The morphological analysis was investigated by Scanning electron microscope (SEM) Inspect F50. The catalysts were characterized by scanning transmission electron microscopy (STEM) (FEI Titian 80-300™) equipped with equipped with energy-dispersive X-ray (EDX) and electron energy loss spectroscopy (EELS). NH_3- and CO_2- TPD studies were performed on AutoChem II-2920 (Micromeritics) chemisorption analyzer. For pretreatment, 0.1 g of samples were heated at 150 °C under helium at a flow rate of 50 mL $min^{-1,}$ and then the samples were saturated with ammonia at 50 °C for 3 h. After purging with helium for 30 min, the TPD study was carried out at a heating rate of 10 °C min^{-1} from 50 to 250 °C. N_2 adsorption-desorption isotherms and pore size distribution were measured at 77 K using a Brunauer-Emmett-Teller (BET) instrument (ASAP 2010, Micromeritics). Before BET measurement, all samples were degassed at 200 °C under reduced pressure for overnight.

3. Results and discussion

3.1. Synthesis and characterization of modulated UiO-66

UiO-66 materials were synthesized using DMF solution contained $ZrCl_4$, BDC, and HCl (1.5 mL) by the modified literature procedure published by Katz *et al.* [8]. The discrete solutions for $ZrCl_4$/ HCl and

Table 1
Profiles of UiO-66 for experimental synthesis, BET, titration, and size.

Sample	Synthesis				BET		Titration			Size
	$ZrCl_4$ (mmol)	BDC (mmol)	HCl (mL)	DMF (mL)	Surface area ($m^2 g^{-1}$)	Pore Volume ($cm^3 g^{-1}$)	Missing Linkers per cluster	Calculated H^+ content from defects[a] (mmol)	Consumed OH^- Content[b] (mmol)	D_{SEM} [c]
UiO-66L	1.62	2.25	1.5	45.0	1394	0.50	1.6	0.317	0.317	580
UiO-66M	1.62	2.25	1.5	22.5	1424	0.51	1.7	0.339	0.337	190
UiO-66S	1.62	2.25	1.5	11.2	1463	0.54	1.8	0.361	0.360	100
UiO-66S (Scale-up)	324	450	300	2200	1459	0.54	–	–	–	100
$UiO\text{-}66_{HCl}$[8,11]	0.54	0.75	1.0	15.0	1580	NA	1.6	0.313[d]	0.311[d]	400

[a] The value was estimated from the formula with the specific number of missing linkers (See Table S2).
[b] The consumed OH- content was calculated using the consumed NaOH titrant between (1) and (3) equivalence point in Fig. 1D.
[c] D_{SEM} was determined by SEM images.
[d] The values were obtained using 0.049 g sample, and others were used 0.05 g of catalysts for titration.

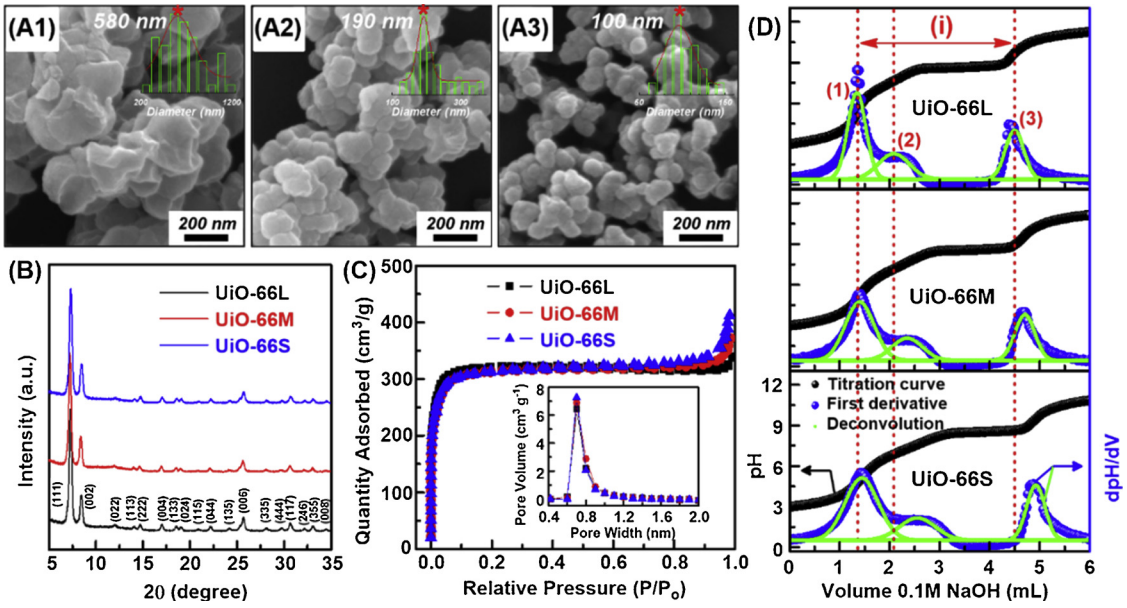

Fig. 1. Representative SEM images of modulated UiO-66 with different sizes: (A1) Large-size (UiO-66L), (A2) Medium-size (UiO-66M), and (A3) Small-size (UiO-66S) (inset: particle size distribution derived from SEM images with Langmuir plot of a solid red line). (B) PXRD patterns and (C) N_2 adsorption/desorption isotherms curves with a pore size distribution of UiO-66L, UiO-66M, and UiO-66S. (D) Acid-base titration curves with first derivative curves and its deconvolution plots using mixed Gaussian-Lorentzian functions.

BDC, respectively, in DMF were mixed by pouring the $ZrCl_4$/ HCl solution into the BDC solution and then heated at 80 °C for 24 h. In order to manipulate the size of UiO-66 particles, the DMF solvent volume was only altered ranging from 45 mL to 11.2 mL, indicating that the total reaction concentration was used as a modulation parameter (Table 1). The controlled three UiO-66 resultants by a reaction concentration were investigated their morphology and size by SEM and indeed exhibited the different size of UiO-66 with 580, 190, and 100 nm, hereafter depending on their sizes denoted by UiO-66L, UiO-66M, and UiO-66S, respectively (Fig. 1A). The SEM image of UiO-66L showed the non-spherical shape along with broad size distribution (Fig. 1A1). In contrast, UiO-66S exhibited the mostly spherical shape with relatively narrow size distribution (Fig. 1A3). The size difference in the synthesized UiO-66 by varying the reaction concentration can be explained by the roles of HCl during the framework that is retarding the hydrolysis of $ZrCl_4$ as well as the deprotonation of BDC [26,32,33]. In particular, increasing the reaction concentration can more facilitate the charge neutrality of Zr cations by promoting abundant Cl anions around Zr cations. In addition, the largely reduced reaction volume (4-times) for UiO-66S relative to the volume for UiO-66L can facilitate the substantially facile scale-up process and also allow higher cost-saving in the synthesis of UiO-66. To confirm this, we performed the ca. 416-times larger-scale reaction than previously reported one by Katz *et al.* [8], resulting in that 98.65 g of the activated UiO-66S was successfully obtained without noticeable degradation in size and BET results compared to those of UiO-66S prepared by a smaller-scale (Table 1).

The PXRD patterns of a series of UiO-66 exhibited that the synthesized materials have isostructure with UiO-66 in addition to suggesting their high crystallinity (Fig. 1B) [38,39]. Fig. 1C displays the N_2 adsorption-desorption isotherms for UiO-66L, UiO-66M, and UiO-66S, exhibiting the surface area of 1394, 1424, and 1463 $m^2 g^{-1}$, respectively. Although the surface area for all UiO-66 materials showed good similarity, one can see that UiO-66S exhibited the highest surface area and sequentially followed by UiO-66M and UiO-66L. The particle size dependent surface area alteration is well consistent with the reported result by Li *et al.* investigating with the NU-1000 Zr(IV)-based MOF, in which the surface area increased according to a particle size decrease (Table 1) [30]. The pore size distribution of all UiO-66 showed the almost similar curve shape, and the peak point was centered at 0.7 nm (Fig. 1C inset). However, the pore volume slightly increased with a decrease of particle size, which was an unexpected result in our knowledge because the pore volume should be the same based on the structure perfection of UiO-66. With regard to a defect structure of MOFs, the previous report by Shearer *et al.* mentioned that the deficient

linkers in the framework can generate an increase of surface area and pore volume [26]. In addition, DeStefano *et al*. also reported defective UiO-66, demonstrating it using BET isotherm curves with observing an increase of surface areas and uphill N_2 adsorption at a high pressure relative to less defective UiO-66, which can well address our BET results [38]. To this end, the changes by defect sites in UiO-66 were highly motivated to consider that the change of the reaction concentration can induce tuning the missing linker density and surface area in the prototypical UiO-66 [26]. Furthermore, we believed that an increase of missing linkers in UiO-66 could afford a high hydrolysis rate by increased accessible and available Lewis acidic Zr moieties.

To confirm our hypothesis concerning tuneable defect sites on the UiO-66 structure, we explored quantifying the missing linker numbers per a cluster particularly employing a potentiometric titration method because we believed that the TGA method based on theoretical calculation using the molecular weight of an UiO-66 unit cell may have deficiency probably derived from types and quantity of oxygenated metals [27]. The potentiometric titration was carried out following the Klet's report [27,28]. Specifically, it was tested by using the UiO-66 dispersed aqueous $NaNO_3$ solution, and then pH of the solution was adjusted to 3 using concentrated HCl. Acid-base titration with synthesized UiO-66 catalysts was performed by dropping the 0.1 M NaOH aqueous solution into the prepared UiO-66 solution (pH 3) till the pH reached ca. 10.5, as shown in Figs. 1D and S1. All UiO-66 samples were tested 3-times, and we used the average values to calculate the number of their missing linkers (Fig. S1). This method has been understood better for quantifying the missing linkers than the approach using TGA albeit the precise identity of defect sites is not clear, but the missing linkers can be replaced with $–OH_2$ and –OH in a term of charge neutralization (Scheme 1) [27]. We should note that the charge compensation arising from missing linkers can be depending on its synthetic protocol and types of modulators [24,26]. In addition, some estimates based on the Klet's report should be discussed as follows: (1) the missing linkers are ranged as high as two per a UiO-66 cluster and (2) the presented protons from defect sites should be probed during titration [27].

In Fig. 1D, all UiO-66 titration curves present the typical three equivalence points assigned with (1), (2), and (3), which correspond to (1) μ_3-OH, (2) $–H_2O$, and (3) –OH based on the estimations and the previous report [27]. The assignment indicated that the titratable protons at (2) and (3) points can be derived from defect sites. The number of missing linkers was calculated using the consumed NaOH titrant between the first equivalence (1) and last equivalence (3) point, denoted with (i) in Fig. 1D. The more extensive consuming of NaOH for the third equivalence indicated that the more massive content of protons is required for titration as well as the more substantial number of missing linkers were presented (Fig. 1D and Table 1). On the basis of the suggested method from the Klet's report, the number of missing linkers per a cluster was evaluated to be approximately 1.6, 1.7, and 1.8, which corresponded to UiO-66L, UiO-66M, and UiO-66S, respectively (Tables 1 and S2) [27]. The resulting values are reasonable in comparison to reported values including the Klet's report ($UiO\text{-}66_{HCl}$: 1.6) (Tables 1 and S1) [27]. The increase of missing linkers according to an increase of reaction concentration can be anticipated by the strong effect of retarding $ZrCl_4$ hydrolysis which can lead to remaining Zr-Cl coordination in the final resultants. The residual Zr-Cl coordination in UiO-66 was confirmed by STEM-EELS elemental mapping and line profile of Zr, C, O, and Cl (Fig. S1D). To avoid the hydrolysis of Zr—Cl, the fresh UiO-66S was applied for STEM-EELS studies. The acquired STEM-EELS elemental mapping image of Cl of fresh UiO-66S demonstrated that Cl (STEM-EDX: 4.2 atomic%) remained throughout UiO-66S (Fig. S1D). Similarly, Han *et al*. also observed the residual Zr—F coordination in the UiO-66 when synthesized it at the high concentration of HF as a modulator [32]. As such, the number of the estimated missing linkers for UiO-66L, UiO-66M, and UiO-66S well demonstrated that altering the reaction concentration can afford to vary the defect site densities as well as the size in the UiO-66 prepared by HCl as a modulator.

3.2. Catalytic evaluation for hydrolysis of MPO in an aqueous solution system

Evaluation of catalytic activity for synthesized UiO-66 catalysts was performed by a model reaction using hydrolysis of MPO which is one of the nerve agent simulants (Fig. 2A) [11,12]. The chemical structure of the MPO simulant has a high similarity to actual nerve agents, and the catalytic reactivity is known as relatively lower than that of actual nerve agents [12,13]. Furthermore, the toxicity is relatively much lower than actual nerve agents. Hence, the MPO has been used for the efficient nerve agent simulant to examine the newly developed catalysts for detoxification of nerve agents. On the basis of previous reports, MPO can be hydrolyzed into *p*-nitrophenol and dimethoxy phosphate by Zr (IV)-based MOFs under the presence of bases including 4-EM and PEI as shown in Fig. 2A [16,31]. The hydrolysis reactions of MPO by synthesized UiO-66 catalysts were performed as followed the *Method 1* in Fig. 2B, specifically the UiO-66 suspension in water was added into the prepared aqueous solution of 4-EM and MPO in a minute. The hydrolysis rates of synthesized UiO-66 catalysts in the catalyzed reaction with MPO were examined by ^{31}P NMR with quantifying the concentration of MPO (*a*) and dimethoxy phosphate (*a'*) (Fig. S2B–S2D). We also confirmed the chemical structure of *p*-nitrophenol and dimethoxy phosphate by ^{1}H NMR after hydrolysis of MPO, displayed in Fig. S2E with structure assignments. The ^{31}P NMR spectra for hydrolysis of MPO by UiO-66S showed a significant reduction of MPO peak at −4.9 ppm and an increase of dimethoxy phosphate peak at 2.9 ppm with an increase of reaction time, indicating the relatively faster kinetics in the hydrolysis of MPO in comparison to that by UiO-66M and UiO-66L (Fig. S2B). Pseudo-first order reaction kinetics were employed to determine the reaction rate constant for the more precise evaluation of the catalytic hydrolysis rate of UiO-66, which can be normalized and described by

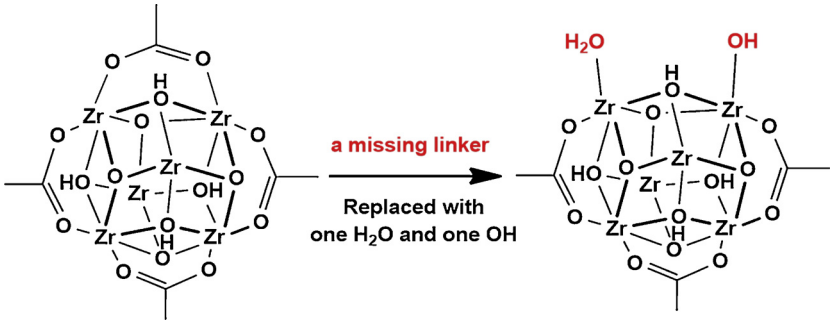

Scheme 1. Schematic illustration of possible defect sites in the UiO-66 cluster derived from a missing linker (the chemical structure of BDC linkers are omitted for clarity of the cluster).

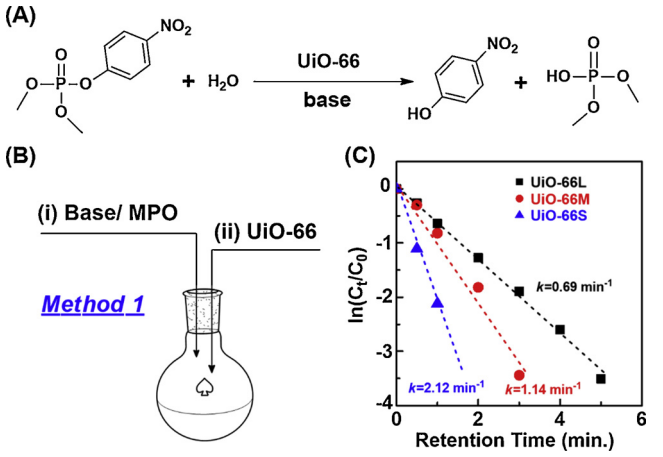

Fig. 2. (A) Scheme for hydrolysis of MPO by UiO-66 in the presence of a base. (B) Proposed catalytic reaction procedure of *Method 1* – (ii) the last addition of UiO-66 catalyst (i) after preparation of a base/MPO mixture (applied for most of the reactions in this study unless otherwise noted). (C) The $\ln(C_t/C_0)$ vs. t plot for hydrolysis of MPO in the presence of catalysts (0.95 μmol) UiO-66L, UiO-66M, and UiO-66S with 4-EM (450 mM) (a linear fit produces dot lines).

Eq. (1):

$$\ln(C_t/C_0) = -kt \quad (1)$$

where C_t is the concentration of MPO at time t, C_0 is the initial concentration of MPO, and k is the pseudo-first-order rate constant [40–42]. The $\ln(C_t/C_0)$ vs. t plot for hydrolysis of MPO catalyzed by UiO-66L, UiO-66M, and UiO-66S (0.95 μmol) exhibited a linear relationship between $\ln(Ct/C_0)$ and t, which well corresponded to pseudo-first order reaction kinetics (Fig. 2C). In addition, UiO-66S showed substantially higher rate constant (2.12 min^{-1}), sequentially followed by UiO-66M (2.12 min^{-1}) and UiO-66L (2.12 min^{-1}) (Table 2, entries 1–3). However, the pseudo-first-order rate constant (k) does not well explain the intrinsic catalytic activity of catalysts because the value does not include the term of the number of reactive sites in the catalyst [42].

The comparative evaluation of synthesized UiO-66 catalysts in the intrinsic catalytic activity was performed by calculation of the TOF which can be defined by Eq. (2) based on relative reports [11,28,29,43]:

$$\text{TOF} = \frac{M_{sub} \times X}{M_{cat} \times t} \quad (2)$$

where M_{sub} and M_{cat} are the amounts of substrate and catalyst, respectively, X is the conversion of the substrate, t is the reaction time. To optimize the conditions for hydrolysis of MPO, the catalyst loading content of UiO-66S, which has an inverse proportional relationship with TOF (Eq. (2)), was reduced to 0.71 and 0.44 μmol from 0.95 μmol, and then TOF values were substantially degraded to 0.235 and 0.014 s^{-1}, respectively (Fig. S3A and Table 2, entries 3–5). When we increase the UiO-66S loading content more than 0.95 μmol, the hydrolysis rate was almost retained, resulting in the reduction in TOF (data is not shown). To this end, the 0.95 μmol catalyst loading content was selected for all reactions hereafter. Table 2 displayed the TOF values of the synthesized UiO-66 catalysts, exhibiting that the UiO-66S showed the higher TOF value (0.548 s^{-1}) than that of UiO-66M (0.239 s^{-1}) and UiO-66L (0.188 s^{-1}) (Table 2, entry 1–3). The TOF value of UiO-66S showed ca. 3-fold higher than that of UiO-66L which is prepared by similar conditions and has similar features to the reported UiO-66 (Table 1) [8,11]. The kinetically faster hydrolysis of MPO by UiO-66S than that of UiO-66L can be explained because the UiO-66S has a smaller particle size (ca. 100 nm) and larger missing linkers (ca. 1.8 per cluster) in comparison to those of UiO-66L (ca. 540 nm and 1.6 per cluster) (Table 1) [28.30]. It is indicative that the UiO-66S has a larger surface area and active Lewis acidic sites than those of UiO-66L. For comparative evaluation, catalytic activity of UiO-66S with *Method 1* in the hydrolysis of MPO was compared with state-of-the-art Zr(IV)-based MOFs including reported UiO-66 (TOF: 0.004 s^{-1}), UiO-66-NH_2 (TOF: 0.15 s^{-1}), UiO-67 (TOF: 0.038 s^{-1}), UiO-67-NH_2 (TOF: 0.044 s^{-1}), and Nu-1000 (TOF: 0.009 s^{-1}), indicating the higher catalytic activity of UiO-66S albeit the reaction process is slightly different (Table 2, entries 3 and 12–16) [12,15,31].

Half-life ($t_{1/2}$) value is also commonly used to determine the catalytic activity of catalysts, in particular, the applications in the MOF-based catalytic reaction for detoxification of chemical warfare agents

Table 2
Profiles for catalytic activities of catalysts under various reaction conditions.

Entry	Method[a]	Catalyst	Catalyst (μmol)	Base	Base (mM)	k[b] (min^{-1})	TOF[c] (sec^{-1})	$t_{1/2}$ (min)	Ref.
1	1	UiO-66L	0.95	4-EM	450	0.688	0.188	1.0	This work
2	1	UiO-66M	0.95	4-EM	450	1.145	0.239	0.6	This work
3	1	UiO-66S	0.95	4-EM	450	2.121	0.548	0.3	This work
4	1	UiO-66S	0.71	4-EM	450	1.342	0.235	0.5	This work
5	1	UiO-66S	0.44	4-EM	450	0.004	0.014[d]	> 40	This work
6	1	UiO-66S	0.95	LPEI10k	0.9 (9 mg)	0.255	0.219	2.7	This work
7	1	UiO-66S	0.95	BPEI10k	0.9 (9 mg)	0.047	0.018	14.7	This work
8	1	UiO-66S	0.95	BPEI0.6k	15 (9 mg)	0.007	0.007[d]	> 60	This work
9	2	UiO-66S	0.95	LPEI10k	0.9 (9 mg)	0.001	0.001[d]	> 60	This work
10	2	UiO-66S	0.95	4-EM	450	0.003	0.003[d]	> 60	This work
11	3	UiO-66S	0.95	4-EM	450	0.006	0.005[d]	> 60	This work
12	4[e]	UiO-66	1.5	4-EM	450	–	0.004	35.0	12
13	4[e]	UiO-66-NH_2	1.5	4-EM	450	–	0.150	1.0	15
14	4[e]	UiO-67	1.5	4-EM	450	–	0.038	4.5	15
15	4[e]	UiO-67-NH_2	1.5	4-EM	450	–	0.044	2.0	15
16	4[e]	NU-1000	1.5	4-EM	450	–	0.009	15.0	12
17	4[e]	NU-1000	1.5	LPEI[f]	3 (7.5 mg)	–	0.017	8.4	31

[a] The catalytic reaction methods are illustrated in Figs. 2B, 4 C, and 6 A.
[b] The reaction rate constant was determined from $\ln(C_t/C_0)$ vs. t plots.
[c] The TOF values were determined at 50% unless otherwise noted.
[d] The TOF values were calculated using conversions at 10 min.
[e] Although the general procedure for the reactions was similar to the *Method 3*, the fresh UiO-66 powder was added to the reaction solution. Meanwhile, the typical *Method 3* uses the prepared suspension of UiO-66 in methanol.
[f] The molecular weight of LPEI is 2500 g mol^{-1}.

(CWA) [12,13,29]. For a first-order reaction, $t_{1/2}$ can be determined by $t_{1/2} = 0.693/k$ [43]. The $t_{1/2}$ value of UiO-66S was calculated to be 0.3 min and sequentially followed by UiO-66M (0.6 min) and UiO-66L (1.0 min) (Fig. S3B). It should be importantly noted that the simple approach of varying the reaction concentration for the synthesis of UiO-66 significantly influenced on tuning the catalytic activity of UiO-66 for the hydrolysis of MPO.

3.3. Feasibility tests with polymeric bases

Recent studies with regard to catalytic reactions of Zr(IV)-based MOFs in detoxification of CWAs suggested that all reagents should be a solid state for the actual application such as protective suits and masks [16,31]. Toward enhanced feasibility with MOF catalysts, the LPEI (solid) was previously proposed for a promising base material, which can alter the liquid type base of 4-EM [16]. In addition, LPEI with a combination of UiO-66 and Nu-1000 allowed the catalytic activities as high as 4-EM performed [16,31]. The preliminary examination toward high feasibility drew our attention into investigating the enhanced feasibility of Zr(IV)-based MOF catalysts for detoxification of CWAs. To this end, the hydrolysis rate of UiO-66S with MPO was examined under the presence of either BPEI0.6k (MW: 600 g mol^{-1}), BPEI10k (MW: 10,000 g mol^{-1}), or LPEI10k (MW: 10,000 g mol^{-1}). The chemical structure of LPEI and BPEI is illustrated in Fig. 3A, and those contained abundant amine sites which can play as a Brønsted base. First, the hydrolysis of MPO with the various loading mass of LPEI10k as a controlled parameter was performed using *Method 1* in the presence of UiO-66S (0.95 μmol) (Figs. 3B and S4A). Fig. 3B shows the MPO hydrolysis conversion at 20 min according to the LPEI10k loading mass which exhibited that an increase of LPEI10k loading mass from 3 to 9 mg allowed uphill conversions. However, the more increase of LPEI10k loading mass than 9 mg led to the reaction saturation as shown in Fig. S4A. Although the combination of UiO-66S and LPEI10k (9 mg) showed lower catalytic activity in the k (0.225 min^{-1}), TOF (0.219 s^{-1}), and $t_{1/2}$ (1.0 min) values in comparison to those by the combination of UiO-66S and 4-EM (k = 2.121 min^{-1}, TOF = 0.548 s^{-1}, and $t_{1/2}$ = 24 s), the values indicated highly enhanced catalytic activity relative to those of reported catalysts with 4-EM or LPEI (2.5k) (Table 2, entries 3, 6, and 12–17). The results can be anticipated because of the intrinsic features of UiO-66S involving the smaller particle size and more extensive active sites than reported one [8,12,27]. In hydrolysis of MPO under the presence of UiO-66S, 9 mg of the PEI loading mass was selected for the optimized conditions in further reactions with PEI.

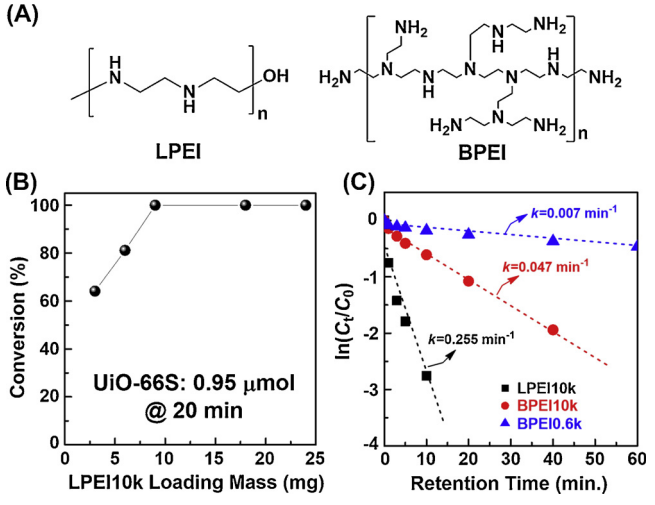

Fig. 3. (A) Chemical structures of linear-type polyethyleneimine (LPEI) and branch-type polyethyleneimine (BPEI). (B) The conversion plot for hydrolysis of MPO by UiO-66S (0.95 μmol) as a function of LPEI10k loading mass and the conversions were determined at 20 min. (C) The ln(C_t/C_0) vs. t plot for hydrolysis of MPO by UiO-66S (0.95 μmol) with the presence of the PEI bases (9 mg) including LPEI10k, BPEI10k, and BPEI0.6k (a linear fit produces dot lines).

We expected that BPEI, which has not been examined so far for MPO hydrolysis and is well soluble in water, can lead to the higher catalytic activity than that obtained from LPEI because LPEI has a lesser solubility in water. With optimized PEI loading mass (9 mg), we performed the hydrolysis reaction with MPO in the presence of BPEI10k or BPEI0.6k, resulting in that catalytic activities were sequentially ordered as follows: LPEI10k ≫ BPEI10k > BPEI0.6k (Figs. 3C and S4B and Table 2, entries 6–8). The acquired results by the presence of PEIs cannot be explained by the reactions with respect to homogeneous and heterogeneous reactions when compared between LPEI10k and BPEI10k [44,45]. In addition, based on Moon's report, the lower molecular weight of LPEI can provide higher catalytic activity in hydrolysis of MPO because of varying the pH (MW2,500: pH 9.2 and MW250,000: pH 7.7) according to the molecular weight of LPEI, which is a highly important parameter for work as a Brønsted base [31]. We considered that the alteration of pH according to the molecular weight of LPEI can be derived from the solubility differences in water because they fixed the introduced amine contents (0.31 mmol) (Fig. S4C). However, although BPEI0.6k and BPEI10k have good solubility in water and their pH values were almost similar as ca. 11.0 and higher than that of LPEI10k (pH 9.0), BPEI10k showed higher catalytic activity than that of BPEI0.6k (Figs. 3C and S4C). From these experimental investigations, we anticipated that good solubility of BPEI as a Lewis base probably facilely chelate the unsaturated Zr(IV) Lewis acid sites which can play as active sites for hydrolysis of MPO based on the reported reaction mechanism [26,28,46].

To explore our hypothesis with regard to the chelation of the active sites on UiO-66, the hydrolysis reaction with MPO was performed according to the loading mass of BPEI0.6k (Figs. 4A and S5). Fig. 4A shows the conversion points of MPO hydrolysis as a function of the BPEI0.6k loading mass, and the points were acquired at 20 min in the conversion vs time plots in Fig. S5A. The conversion point at 6 mg loading of BPEI0.6k exhibited the highest conversion (72.7%), and then the conversion was abruptly downhill up to 16.3% at the 12 mg loading mass. The more significant loading of the BPEI0.6k up to 24 mg led to a slight increase in the conversion (27.3%). From these results by varying the BPEI0.6k loading mass, we found that the trend of the conversion plot can be associated with a reduction of active sites by the reactions between BPEI Lewis base and UiO-66S Lewis acid sites. Furthermore, the slight enhancement of the conversion with an increase of the BPEI0.6k loading mass from 12 mg can be expected because of the hydrolysis reaction by free BPEI0.6 after over-saturation for active sites of UiO-66S.

To confirm the hypothesis of the catalytic reaction by free BPEI, we employed a hot-filtration method, which is well known to investigate the heterogeneous catalytic reaction [41]. We selected two conversion points in Fig. 4A such as 9 mg for the near saturation point and 24 mg for over-saturation point. The hydrolysis reactions with the different BPEI0.6k loading mass (9 mg vs. 24 mg) were performed, and the conversions were monitored by ^{31}P NMR (Fig. 4B). After the reaction began, the reaction solutions were filtered out at the 20 min point to remove the UiO-66S. We observed the important results to well prove our hypothesis (Fig. 4B). The near saturation point (9 mg) led to the excellent retention in the reaction conversion after hot-filtration. In contrast, the over-saturation condition (24 mg) exhibited consciously increased in the conversion after hot-filtration (Fig. 4B). This investigation suggested that the presence of BPEI can degrade the catalytic activity of UiO-66S because of the presence of BPEI onto the UiO-66S as well as BPEI can play as a catalyst for the hydrolysis of MPO.

Although we indirectly found the PEI may react with UiO-66S by the acid-base reaction, more clarified results are required to bring a rational understanding of reduced catalytic activity by the active site

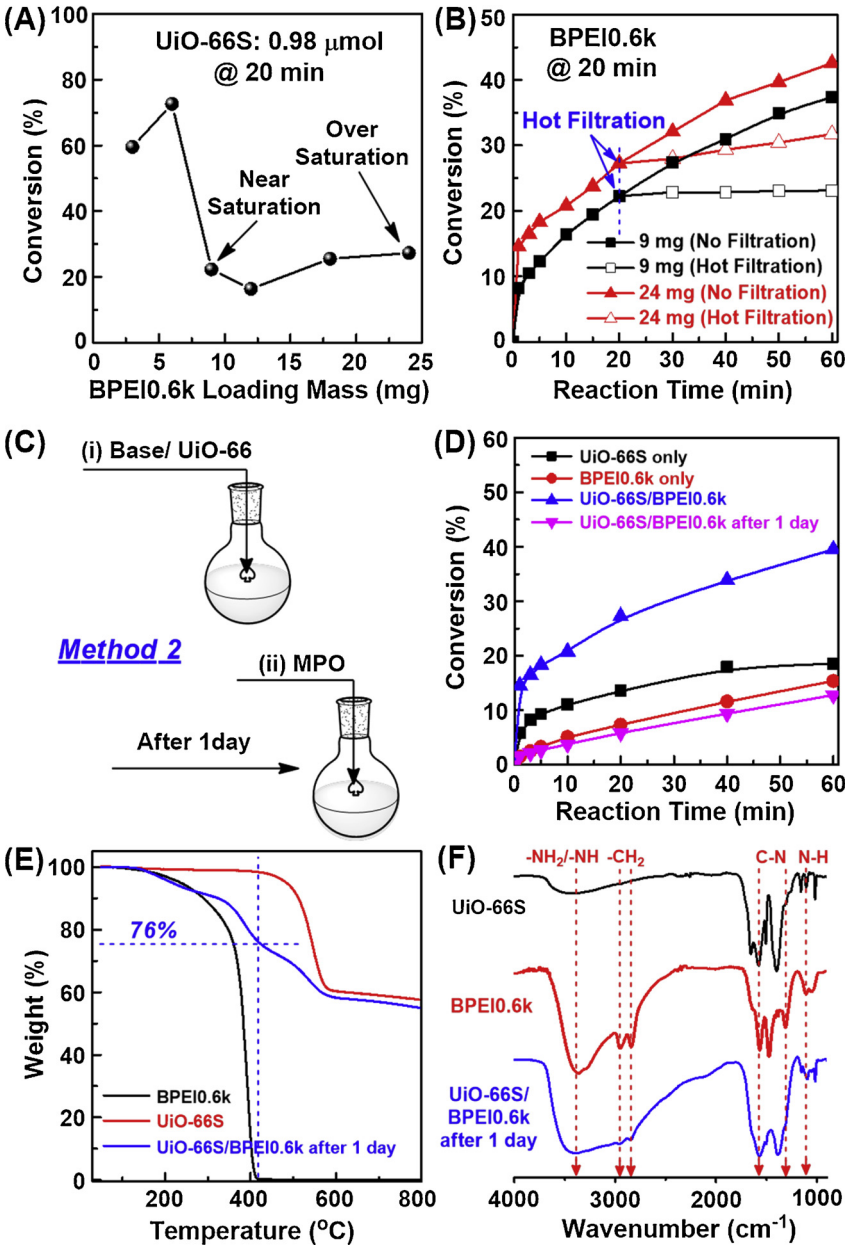

Fig. 4. (A) The conversion plot for hydrolysis of MPO by UiO-66S (0.95 μmol) as a function of BPEI0.6k loading mass and the conversions were determined at 20 min (See Fig. S5). (B) Hydrolysis profiles of MPO by UiO-66S (0.95 μmol) in the presence of 9 or 24 mg of BPEI0.6k, tested with and without hot filtration at 20 min. (C) Proposed catalytic reaction procedure of *Method 2* – (ii) the last addition of MPO (i) after taking 1 day for a mixture of base and UiO-66. (D) Hydrolysis profiles of MPO by UiO-66S only (0.95 μmol), BPEI0.6k only (24 mg), UiO-66S (0.95 μmol) with BPEI0.6k (24 mg) using *Method 1*, and UiO-66S (0.95 μmol) with BPEI0.6k (24 mg) using *Method 2*, respectively. (E) TGA curves and (F) FT-IR spectra of BPEI0.6k, UiO-66S, and the UiO-66S/BPEI0.6k mixture after 1 day (Assignments by dot lines are based on the BPEI structure and the peaks at 1593/1395 and 1510 cm^{-1} corresponded to asymmetric/symmetric COO− stretching and C=C benzene ring of UiO-66S, respectively) [32]. (For interpretation of the references to colour in this figure legend, the reader is referred to the web version of this article.)

chelation phenomenon. In addition, when we consider the aspects of the long-term storages and the ready-to-use state for actual applications of real-time detoxification for CWAs, the stable reactivity of Zr(IV)-based MOF catalysts are highly significant. To this end, we performed the reaction for hydrolysis of MPO with a new method (*Method 2*). Specifically, the MPO solution was added to the prepared BPEI and UiO-66 aqueous solution after one day as illustrated in Fig. 4C. This approach denotes giving the retention time for the reaction between BPEI0.6k and UiO-66S. We compared the catalytic activities for UiO-66S only, BPEI0.6k only, UiO-66S/BPEI0.6k with *Method 1*, and UiO-66S/BPEI0.6k with *Method 2* (Fig. 4D). The hydrolysis of MPO by UiO-66S only and BPEI0.6k only led to an increase in the reaction conversion with increasing the retention time. This catalytic behavior well addresses the rise of conversion in the hot-filtration reactions (24 mg) (Fig. 4B). The result by a UiO-66S/BPEI0.6k mixture with *Method 2* showed substantial degradation in catalytic activity ($k = 0.0021\ min^{-1}$) in comparison to the result acquired by a UiO-66S/BPEI0.6k mixture with *Method 1* ($k = 0.0070\ min^{-1}$), even lower than that of BPEI0.6k only ($k = 0.0026\ min^{-1}$) (Figs. 4D and S5B). These comparisons also strongly indicated that BPEI0.6k could make a reaction with UiO-66S and then disturb the hydrolysis reaction with MPO by passivation of the UiO-66S surface. To understand our suggestion with respect to passivation of Lewis acid sites by BPEI, the comparative examination of acid-base characteristics of UiO-66S and UiO-66S/BPEI0.6k (prepared by Method 2 without MPO) was performed by NH_3- and CO_2-TPD (Fig. S6A and B). The scanning temperature range was determined by concerning the degradation point of the tested materials in the TGA analysis, where we also confirmed the crystal structure of UiO-66S was not changed before and after TPD tests (Fig. S6C). The NH_3-TPD spectrum of UiO-66S was significantly changed in the shape and intensity after the presence of BPEI0.6k (Fig. S6A). In particular, the strong acidic site of UiO-66S exhibited relatively noticeable reduction relative to the intensity of the weak acidic site. We also found that CO_2 desorbed spectrum of UiO-66S/BPEI0.6k showed the new peak at 100.3 °C, which can be assigned to the weaker basic site in comparison to that of UiO-66S (Fig. S6B) [47]. It is anticipated that the weaker basic site is ascribed to the amine groups of BPEI. These changes in acid-base sites by the presence of BPEI0.6k can explain the

substantial degradation in the catalytic activity of UiO-66 when coupled with BPEI in the MPO hydrolysis reaction.

To confirm the introduced BPEI0.6k content onto UiO-66S, we measured TGA with BPEI0.6k, UiO-66S, and the UiO-66S/BPEI0.6k mixture sample after one day (*Method 2*). To obtain the UiO-66S/BPEI0.6k after one day sample, we obtained the precipitates from the *Method 2* reaction solution by filtration and then performed rinsing and sonication with methanol for several times to remove the free BPEI0.6k. The introduced BPEI0.6k content onto UiO-66S was calculated to be 24 wt% by the weight difference of the UiO-66S/BPEI0.6k after one day sample at 416 °C, which is a critical point for 100% thermal degradation of BPEI0.6k and almost 100% retention of UiO-66S (Fig. 4E, guided by blue dot lines) [48]. The FT-IR spectrum of the UiO-66S/BPEI0.6k after one day sample revealed that BPEI0.6k was clearly introduced onto the UiO-66S with observing representative peaks of BPEI at 3377, 2955/2836, 1564/1312, 1470, and 1115/1049 cm^{-1}, which corresponded to $-NH_2$/−NH bending, asymmetric/symmetric $-CH_2$ stretching, C−N stretching, and N−H wagging of BPEI, respectively [49]. As such, these broad investigations for the effects of BPEI on hydrolysis of MPO catalyzed by UiO-66 suggested that the long-term retention of the UiO-66S/BPEI mixture cannot have good feasibility toward applying to the actual applications.

Based on the investigations with BPEI, we also consider that the UiO-66/LPEI mixture cannot also avoid the downhill catalytic activity after the long-term retention in the mixture state. To confirm the long-term stability of the catalytic activity, *Method 2* with UiO-66S and LPEI10k was applied for the hydrolysis reaction of MPO. Fig. 5 showed that LPEI10k does not have catalytic property for hydrolysis of MPO. Importantly, one-day retention of the UiO-66S/LPEI10k mixture led to a conspicuously substantial degradation in its catalytic activity (TOF = 0.001 s^{-1}) relative to that obtained by *Method 1* (TOF = 0.219 s^{-1}) as we expected (Fig. 5A and Table 2, entries 6 and 9). In addition, the rate constant value obtained by *Method 2* exhibited a 255-fold decrease in comparison to the value obtained by *Method 1* (Fig. S7). The method-dependent catalytic behaviors can be demonstrated by NH_3- and CO_2-TPD studies (Fig. S6). The alteration in NH_3 and CO_2 desorption curves of UiO-66S/LPEI10k in comparison to those of UiO-66S were almost consistent with that observed in the spectra by UiO-66S/BPEI0.6k albeit UiO-66/LPEI10k exhibited the relatively higher intensity than those of UiO-66S/BPEI0.6k because it is probably the higher content of integrated BPEI0.6k (ca. 24%) than that of LPEI10k (ca. 11%).

TGA was employed for the determination of the quantity of introduced LPEI10k onto UiO-66S. The TGA sample was prepared by washing and sonication of precipitates with an excess of methanol after the *Method 2* reaction with UiO-66S and LPEI10k. The TGA curves suggested that 11 wt% of LPEI10k remained on UiO-66S, which was calculated by weight change of the UiO-66S/LPEI10k after one day sample at 416 °C (Fig. 5B). In addition, it should be noted that the introduced LPEI10k content was indeed lower than BPEI0.6k (24 wt%). Furthermore, the FT-IR spectrum of the UiO-66S/LPEI10k after one day sample confirmed indeed the presence of LPEI10k onto UiO-66S with observing representative peaks of LPEI at 3430, 2915/2846, 1572/1317, 1470, and 1156/1133 cm^{-1}, which corresponded to −NH bending, asymmetric/symmetric $-CH_2$ stretching, C−N stretching, and N−H wagging of LPEI, respectively [49]. These extensive investigations using the UiO-66 composite with LPEI suggested that the LPEI candidate as an alternative for 4-EM does not have good feasibility for the applications in the real-time detoxification for CWA.

3.4. Catalytic evaluation in a polymer composite system at various relative humidity and temperature conditions

Although the above catalytic system showed excellent detoxification of MPO in the aqueous solution, the catalytic system based on all-solid-state such as a polymer composite could give better feasibility for the actual military applications such as protective suits and equipment. For this purpose, the cotton fabric was used as a support, and then the suspension of UiO-66S and LPEI10k in methanol was coated on the cotton fabric by a drop-casting method (Fig. 6A1 and A2). The MPO nerve agent simulant was introduced onto the surface of the UiO-66S/LPEI10k composite coated cotton fabric, and then MPO hydrolysis was examined by changing two parameters, the relative humidity and the temperature to create actual atmospheric conditions (Fig. 6A3). [50] The humidity is the most important for hydrolysis reactions because the reaction cannot be allowed without water [51–53]. In addition, the temperature can provide the energy for overcoming the activation energy for substitution reaction between H_2O and MPO in the ligation with Zr(IV) because the binding free energy for Zr-MPO is relatively higher than that for the interaction between UiO-66 and MPO on the basis of the DFT results by Mondloch *et al.* [29,54].

The control of humidity as a reaction parameter suggested that the hydrolysis of MPO is indeed the humidity-dependent reaction with exhibiting a substantial conversion difference in the initial reaction step (Fig. 6B). Moreover, the reaction conversions seem to be saturated during the reaction. It can be anticipated because of a decrease of reactive sites on UiO-66S by chelating with LPEI10k under the presence of high humidity. The reason can be indirectly confirmed by observing a shift of the onset-point to the higher reaction time from 5 h (at 99% RH) to 13 h (at 65% RH) with decreasing the humidity (the onset-point denoted the saturation point of the reaction conversion in Fig. 6B). The plots for hydrolysis of MPO according to the temperature changes from 15 °C to 40 °C suggested that a temperature parameter is lesser effective for the hydrolysis reaction than that by humidity changes albeit the

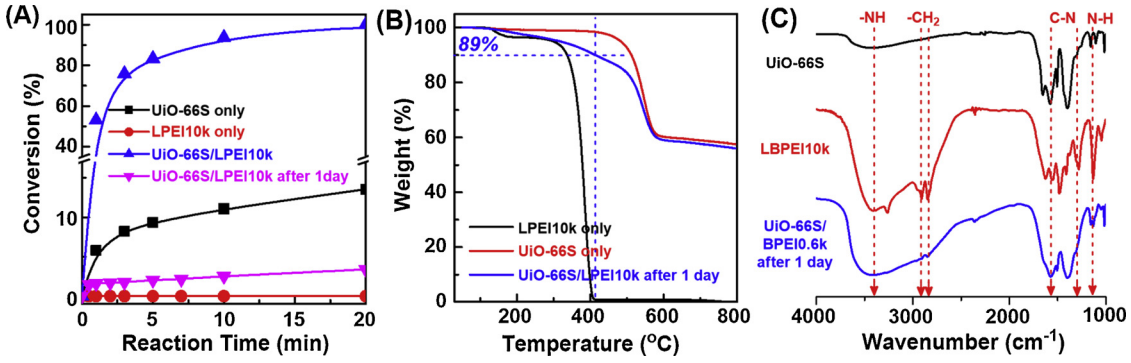

Fig. 5. (A) Hydrolysis profiles of MPO by UiO-66S only (0.95 μmol), LPEI10k only (9 mg), UiO-66S (0.95 μmol) with LPEI10k (9 mg) using *Method 1*, and UiO-66S (0.95 μmol) with LPEI10k (9 mg) using *Method 2*. (B) TGA curves and (F) FT-IR spectra of LPEI10k, UiO-66S, and the UiO-66S/LPEI10k mixture after 1 day (assignments by dot lines are based on the LPEI structure and the peaks at 1593/1395 and 1510 cm^{-1} corresponded to asymmetric/symmetric COO− stretching and C=C benzene ring of UiO-66S, respectively) [32].

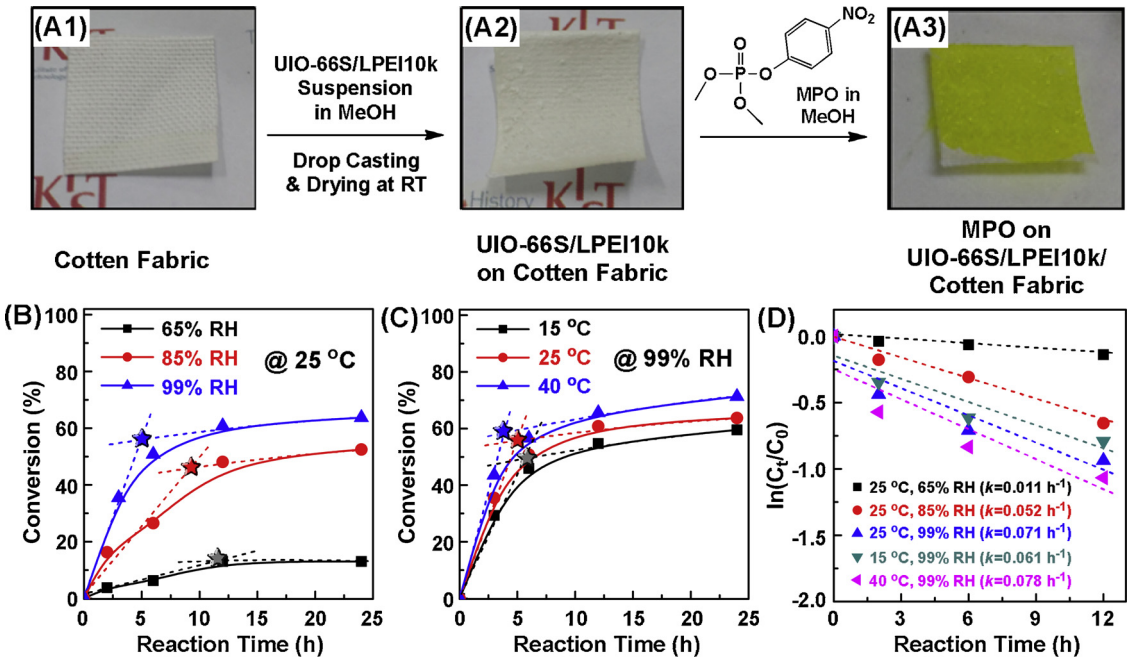

Fig. 6. Representative photographs for a controlled hydrolysis reaction of MPO as a function of either humidity or temperature. (A1) 1 × 1 cm^2-sized cotton fabric, (A2) UiO-66S/LPEI10k composite-coated cotton fabric prepared by drop-casting with methanol suspension of UiO-66S /LPEI10k and then dried at RT, (A3) presence of diluted MPO (0.253 mmol mL^{-1}) in methanol onto the UiO-66S/LPEI10k composite-coated cotton fabric. Hydrolysis profiles of MPO by UiO-66S (B) with different humidity at 25 °C and (C) with the different temperature at 99% RH (the star marks denote the onset-point for the saturated reactivity). (D) The $\ln(C_t/C_0)$ vs. *t* plot for hydrolysis of MPO with controlled conditions.

increasing temperature allowed the enhanced hydrolysis rate (Fig. 6C). In addition, the change of the onset-points according to the temperature was not shown the substantial difference relative to the that by humidity (Fig. 6B and C). For comparative evaluation, the $\ln(C_t/C_0)$ vs. *t* plots were employed, and the substantially saturated point (at 24 h) in the conversion changes were ignored for reasonable calculation of *k* by pseudo-first order reaction kinetics (Eq. (1)). The resulting *k* values according to the different conditions of temperature and humidity suggested that the condition at 40 °C and 99% RH is the optimized condition for hydrolysis of MPO. The *k* value (0.078 h^{-1}) at the optimized condition is ca. 200-fold lower than the value (15.3 h^{-1}) acquired by the solution sate system (Table 2, entry 6). In contrast, the result by *Method 2* ($k = 0.06\ h^{-1}$) is almost consistent with the result at the optimized condition ($k = 0.078\ h^{-1}$) albeit the *Method 2* performed in the water solution system (Table 2, entry 9). It is indicative that the approach for the UiO-66S/LPEI10k composite coating system has low feasibility as well as the catalytic activity in the combination of UiO-66S and LPEI10k are highly dependent on the reaction process. As such, the LPEI10k coated UiO-66S does not have excellent catalytic activity for hydrolysis of MPO regardless of the state of the reaction conditions.

3.5. Catalytic evaluation with different reaction processes

From the feasibility tests with PEIs, we also considered whether the presence of 4-EM in *Method 2* reaction can maintain the intrinsic catalytic activity of UiO-66S or not. In addition, if 4-EM also reacts with Lewis acid sites on UiO-66S because of high pH value of 4-EM (10.9), how fast it is to make the reaction. To investigate those two issues, we suggest *Method 3*, in which the MPO solution was added to the prepared suspension containing UiO-66S and 4-EM in a minute, as illustrated in Fig. 7A. With a combination of UiO-66S and 4-EM, we performed hydrolysis of MPO using suggested three different methods in this study (Fig. 7B). The results by *Method 2* and *3* indicated that 4-EM immediately affects to the catalytic activity of UiO-66S because we observed the similar *k* (0.003 and 0.006 min^{-1}, respectively) and TOF (0.003 and 0.005 s^{-1}, respectively) values regardless of the retention time after preparation of the UiO-66S and 4-EM mixture (Fig. S8 and Table 2, entries 10 and 11). These values by *Method 2* and 3 exhibited substantial degradation of the catalytic activity in comparison to the results by *Method 1*, shown explicitly that TOF values were downhill ca. 200- and 100-times in TOF, respectively (Table 2, entries 3, 10 and 11). To confirm the introduction of 4-EM into UiO-66S by *Method 2* and *3* as shown in the case of PEI/UiO-66, TGA and FT-IR analysis were performed. However, the low quantity introduction and small molecular weight of 4-EM rendered difficulty in its characterization. We performed the STEM-EELS elemental mapping of N (green) of UiO-66S which is prepared by several rinsing and drying steps after the treatment based on *Method 2* without MPO (Fig. 7C). We anticipated that the STEM-EELS study may be a good solution to detect the minuscule quantity of 4-EM and evaluate its distribution. Although the N element was not fully covered the UiO-66S, we observe the N (STEM-EDX: 2.1 atomic%) element throughout UiO-66S, suggesting that 4-EM probably introduced to the UiO-66S because the chemical structure of UiO-66S does not contain the N element (Fig. 7C and Scheme 1). Furthermore, the NH_3-TPD study also provided the good evidence for the presence of 4-EM to the UiO-66S, in which the intensity of acidic sites on UiO-66S was significant downhill after mixing UiO-66S with 4-EM for 1 day (Fig. S6A). As such, the use of 4-EM as a base material with UiO-66 catalysts for composite materials will still be challenging to have good feasibility because of the suggested acid-base reaction leading to substantially reduced catalytic activity after its long-term storage.

3.6. Computational calculations for the reaction mechanism

For a further understanding of the substantial reduction in catalytic activity of the MPO hydrolysis performed by *Method 2*, we carried out quantum chemical calculations at the density functional theory (DFT) calculation level. Fig. S9 shows all geometries of the MOF-agent complexes optimized in the present DFT calculations, and free energy changes for the relevant reactions are presented in Table S3. The substitution reaction free energy of MPO by 4-EM on UiO-66 (sixth reaction in Table S3) is slightly endergonic by 7.5 kcal mol^{-1}, which indicates

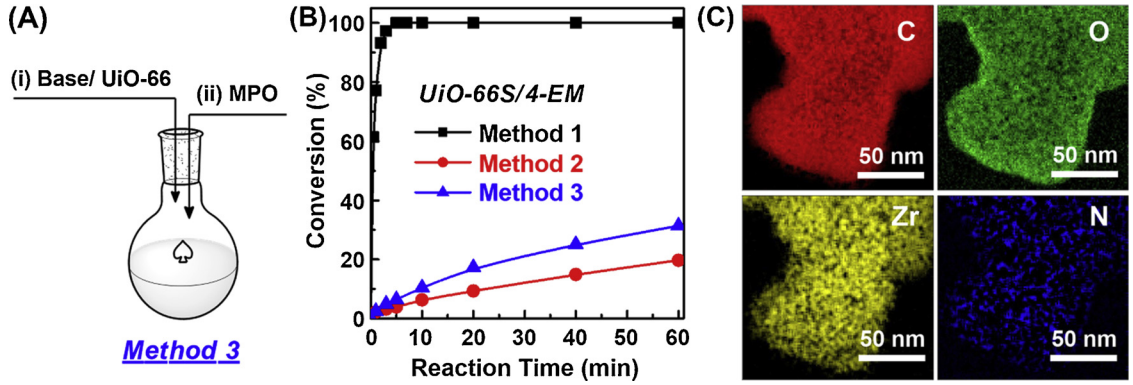

Fig. 7. (A) Proposed catalytic reaction procedure of *Method 3* – (ii) the last addition of MPO (i) after preparation of a base/UiO-66 mixture. (B) Hydrolysis profiles of MPO by a combination of UiO-66S (0.95 μmol) and 4-EM (450 mM) with different reaction methods (See Figs. 2B and 4 C). (C) STEM-EELS elemental mapping of C, O, Zr, and N of UiO-66S after treatment with 4-EM based on *Method 2*.

that the reaction would not readily occur under the atmosphere environment. The simulation result can support the experimental observations that *Methods 2* and *3* show the low reaction rate. When 4-EM passivates the defect sites in UiO-66, it is difficult for the MPO substitution reaction to occur for the post catalysis. Here, one question can be raised: why *Method* 1 shows a fast reaction rate although MPO has the lower binding energy (16 kcal mol^{-1}) in UiO-66 than H_2O (29.5 kcal mol^{-1}). Although the binding free energy is larger for an H_2O molecule, the environment is water itself, which means that substitution of the attached H_2O molecule happens so frequently. Energetically, the substitution activation of MPO by H_2O may be harder than that of the reverse situation, but the explicit values were not possible in this work due to the vast calculation amount. After formation of a chemical bond between MPO and UiO-66, the activation of this relatively large molecule to be detached may not be so easy when compared to the detachment of H_2O molecule. There is an interesting point to be noticeable from the reaction in the last row of Table S3. It is a consensus that the catalysis of MPO on UiO-66 would happen on one Zr metal atom defect site. As seen in Fig. S9E, however, the stable geometry of MPO + H_2O on UiO66 has a bond between P on MPO and OH groups on the other conjugate defect site on UiO66. Hence, we can obtain an insight that the hydroxyl group on other Zr site has an important role in the detoxification reaction process contrary to the previous mechanism. The proposed new reaction mechanism is represented in Fig. 8.

All our extensive investigations with various reaction methods and organic base candidates along with the reaction energy prediction by DFT suggest that the long-term storage of together with MPO and bases including 4-EM and PEI can lead to substantial downhill catalytic activity in the hydrolysis of MPO. To solve these issues, development of new polymer base materials to provide the highly stable catalytic activity to Zr-based MOF catalysts as well as investigations for new processing of catalytic reactions, for example, separated storage of catalyst and base and affording fast mixing when exposed CWAs, remains as essential challenges for the suggested potential applications.

4. Conclusions

For high-performance catalysis, the modulated UiO-66 catalysts with three different defect density and particle size were successfully synthesized by adjusting the hydrolysis of $ZrCl_4$ and deprotonation of BDC. The reduced solvent volume led to the most active UiO-66 catalyst (UiO-66S) with the smallest UiO-66 particle size (ca. 100 nm) and the highest defect density (1.8 per a cluster), which are favorable properties in Lewis acid-catalyzed reactions in addition to providing an efficient scale-up synthesis. The UiO-66S indeed showed the substantially enhanced hydrolysis rate for MPO under the presence of the 4-EM base (TOF: 0.547 s^{-1}) in comparison to that of UiO-66L (low defect density: 1.6 per a cluster, 1.88 s^{-1}). With UiO-66S, we investigated its feasibility under the presence of polymer bases including LPEI and BPEI. However, we found that the catalytic performance was significantly dependent on the content of PEI in the MPO hydrolysis reactions because of the strong and fast coordinative ligation between Lewis acid Zr sites in UiO-66 and Lewis base amine sites in PEIs. Furthermore, we prepared all-soli-state catalytic system based on the polymer composite of UiO-66S/LPEI10k on cotton fabrics to examine the MPO hydrolysis reaction with varying relative humidity and temperature conditions instead of the previous aqueous solution condition to show the feasibility for the actual military applications including protective suits and equipment. At the optimized conditions of 40 °C and 99% RH, the *k* value exhibited 0.078 h^{-1} which was slightly higher than the result by the aqueous solution process using *Method 2*, albeit it was still much lower value than the result by *Method 1* (15.3 h^{-1}). We found that the catalytic activity in the combination of UiO-66S and LPEI10k was highly dependent on the reaction process because of the low stability of reactive Lewis acidic sites by the interaction with strong bases. Based

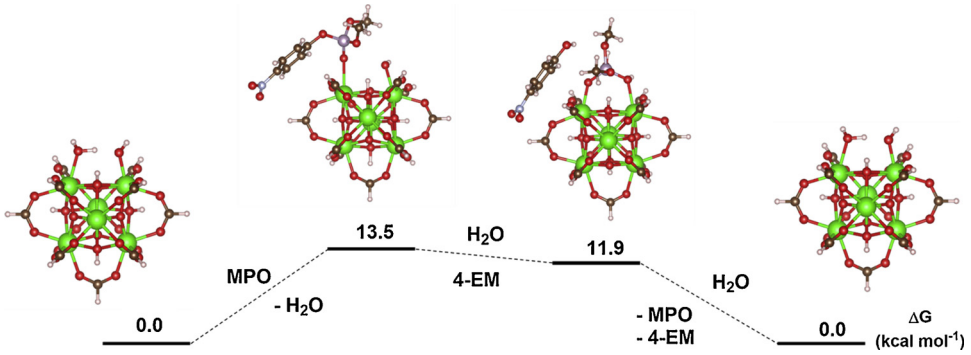

Fig. 8. Reaction energies calculated by DFT for 4-EM binding on UiO-66 and the substitution of 4-EM with MPO. Color codes of the atoms are Zr = green, O = red, H = white, C = brown, P = dark-pink and N = light-purple. (For interpretation of the references to colour in this figure legend, the reader is referred to the web version of this article.)

on the investigations with PEI, we also found that 4-EM affected the reactivity of UiO-66, which could also be explained by the acid-base interaction. To confirm the reactivity changes by chelation of organic bases, quantum chemical calculations at the density functional theories (DFT) calculation level were performed. The substitution reaction of 4-EM with MPO at the Zr sites in UiO-66 was an endergonic reaction (7.5 kcal mol^{-1}), which supported that the reaction was difficult under ambient conditions. Our extensive experimental and computational investigations suggest that development of rationally designed new base materials to incorporate with Zr(IV)-based MOF catalysts are still challenging. Additionally, substantial attention should be considered towards investigating the reasonable processing of catalytic reactions to afford the stable and uniform catalytic reactions in the use of Zr(IV)-based MOF catalysts incorporating with base materials

Acknowledgments

This work was supported by the National Research Council of Science & Technology (NST) grant by the Korea government (MSIP) (No. CMP-16-04-KITECH) and partially supported by R&D Convergence Program of Ministry of Science, ICT and Future Planning, National Research Council of Science & Technology (No. CRC-14-1-KRICT). SSH acknowledges a financial support by the Creative Materials Discovery Program through National Research Foundation of Korea (NRF-2016M3D1A1021140).

Appendix A. Supplementary data

Supplementary material related to this article can be found, in the online version, at doi:https://doi.org/10.1016/j.apcatb.2019.01.033.

References

[1] H. Furukawa, K.E. Cordova, M. O'Keeffe, O.M. Yaghi, The chemistry and applications of metal-organic frameworks, Science 341 (2013) 1230444.
[2] X.-Y. Han, D.-L. Pan, H. Chen, X.-B. Bu, Y.-X. Gao, H. Gao, Y. Tian, G.-S. Li, G. Wang, S.-L. Cao, C.-Q. Wan, G.-C. Guo, A methylthio-functionalized-MOF photocatalyst with high performance for visible-light-driven H_2 evolution, Angew. Chemie - Int. Ed. 57 (2018) 9864–9869.
[3] K.Y. Cho, H. An, X.H. Do, K. Choi, H.G. Yoon, H.-K. Jeong, J.S. Lee, K.-Y. Baek, Synthesis of amine-functionalized ZIF-8 with 3-amino-1,2,4-triazole by post-synthetic modification for efficient CO_2-selective adsorbents and beyond, J. Mater. Chem. A 6 (2018) 18912–18919.
[4] X. Li, Z. Le, X. Chen, Z. Li, W. Wang, X. Liu, A. Wu, P. Xu, D. Zhang, Graphene oxide enhanced amine-functionalized titanium metal organic framework for visible-light-driven photocatalytic oxidation of gaseous pollutants, Appl. Catal. B 236 (2018) 501–508.
[5] A.G. Slater, A.I. Cooper, Function-led design of new porous materials, Science 348 (2015) 8075.
[6] Y.-B. Huang, J. Liang, X.-S. Wang, R. Cao, Multifunctional metal–organic framework catalysts: synergistic catalysis and tandem reactions, Chem. Soc. Rev. 46 (2017) 126–157.
[7] M. Kandiah, M.H. Nilsen, S. Usseglio, S. Jakobsen, U. Olsbye, M. Tilset, C. Larabi, E.A. Quadrelli, F. Bonino, K.P. Lillerud, Synthesis and stability of tagged UiO-66 Zr-MOFs, Chem. Mater. 22 (2010) 6632–6640.
[8] M.J. Katz, Z.J. Brown, Y.J. Colón, P.W. Siu, K.A. Scheidt, R.Q. Snurr, J.T. Hupp, O.K. Farha, A facile synthesis of UiO-66, UiO-67 and their derivatives, Chem. Commun. 49 (2013) 9449.
[9] X. Xu, R. Liu, Y. Cui, X. Liang, C. Lei, S. Meng, Y. Ma, Z. Lei, Z. Yang, PANI/FeUiO-66 nanohybrids with enhanced visible-light promoted photocatalytic activity for the selectively aerobic oxidation of aromatic alcohols, Appl. Catal. B 210 (2017) 484–494.
[10] J. Qiu, X. Zhang, Y. Feng, X. Zhang, H. Wang, J. Yao, Modified metal-organic frameworks as photocatalysts, Appl. Catal. B 231 (2018) 317–342.
[11] M.J. Katz, J.E. Mondloch, R.K. Totten, J.K. Park, S.T. Nguyen, O.K. Farha, J.T. Hupp, Simple and compelling biomimetic metal-organic framework catalyst for the degradation of nerve agent simulants, Angew. Chemie - Int. Ed. 53 (2014) 497–501.
[12] S.Y. Moon, Y. Liu, J.T. Hupp, O.K. Farha, Instantaneous hydrolysis of nerve-agent simulants with a six-connected zirconium-based metal-organic framework, Angew. Chem. Int. Ed. 54 (2015) 6795–6799.
[13] S.Y. Moon, G.W. Wagner, J.E. Mondloch, G.W. Peterson, J.B. DeCoste, J.T. Hupp, O.K. Farha, Effective, facile, and selective hydrolysis of the chemical warfare agent VX using Zr6-based metal-organic frameworks, Inorg. Chem. 54 (2015) 10829–10833.
[14] Z. Hu, D. Zhao, De facto methodologies toward the synthesis and scale-up production of UiO-66-type metal–organic frameworks and membrane materials, Dalton Trans. 44 (2015) 19018–19040.
[15] M.J. Katz, S.-Y. Moon, J.E. Mondloch, M.H. Beyzavi, C.J. Stephenson, J.T. Hupp, O.K. Farha, Exploiting parameter space in MOFs: a 20-fold enhancement of phosphate-ester hydrolysis with UiO-66-NH_2, Chem. Sci. 6 (2015) 2286–2291.
[16] T. Islamoglu, A. Atilgan, S.-Y. Moon, G.W. Peterson, J.B. Decoste, M. Hall, J.T. Hupp, O.K. Farha, Cerium(IV) vs Zirconium(IV) based metal-organic frameworks for detoxification of a nerve agent, Chem. Mater. 29 (2017) 2672–2675.
[17] Z. Wang, S.M. Cohen, Postsynthetic modification of metal–organic frameworks, Chem. Soc. Rev. 38 (2009) 1315.
[18] M. Kim, J.F. Cahill, H. Fei, K.A. Prather, S.M. Cohen, Postsynthetic ligand and cation exchange in robust metal-organic frameworks, J. Am. Chem. Soc. 134 (2012) 18082–18088.
[19] S.M. Cohen, Postsynthetic methods for the functionalization of metal-organic frameworks, Chem. Rev. 112 (2012) 970–1000.
[20] Z. Zhang, L. Zhang, L. Wojtas, P. Nugent, M. Eddaoudi, M.J. Zaworotko, Templated synthesis, postsynthetic metal exchange, and properties of a porphyrin-encapsulating metal-organic material, J. Am. Chem. Soc. 134 (2012) 924–927.
[21] M. Kassai, R. Teopipithaporn, K.B. Grant, Hydrolysis of phosphatidylcholine by cerium(IV) releases significant amounts of choline and inorganic phosphate at lysosomal pH, J. Inorg. Biochem. 105 (2011) 215–223.
[22] R.A. Moss, K.G. Ragunathan, Metal cation micelle mediated hydrolysis of phosphonic acid esters, Langmuir 15 (1999) 107–110.
[23] R.A. Moss, H. Morales-Rojas, S. Vijayaraghavan, J. Tian, Metal-cation-mediated hydrolysis of phosphonoformate diesters: chemoselectivity and catalysis, J. Am. Chem. Soc. 126 (2004) 10923–10936.
[24] Z. Fang, B. Bueken, D.E. De Vos, R.A. Fischer, Defect-engineered metal-organic frameworks, Angew. Chem. Int. Ed. 54 (2015) 7234–7254.
[25] S. Ling, B. Slater, Dynamic acidity in defective UiO-66, Chem. Sci. 7 (2016) 4706–4712.
[26] F. Vermoortele, B. Bueken, B. Van De Voorde, M. Vandichel, K. Houthoofd, A. Vimont, M. Daturi, M. Waroquier, V. Van Speybroeck, C.E. Kirschhock, et al., Synthesis modulation as a tool to increase the catalytic activity of MOFs: the unique case of UiO-66 (Zr), J. Am. Chem. Soc. 66 (2013) 0–3.
[27] R.C. Klet, Y. Liu, T.C. Wang, J.T. Hupp, O.K. Farha, Evaluation of Brønsted acidity and proton topology in Zr- and Hf-based metal–organic frameworks using potentiometric acid–base titration, J. Mater. Chem. A 4 (2016) 1479–1485.
[28] M.J. Katz, R.C. Klet, S.-Y. Moon, J.E. Mondloch, J.T. Hupp, O.K. Farha, One step backward is two steps forward: enhancing the hydrolysis rate of UiO-66 by decreasing [OH–], ACS Catal. 5 (2015) 4637–4642.
[29] J.E. Mondloch, M.J. Katz, W.C. Isley, P. Ghosh, P. Liao, W. Bury, G.W. Wagner, M.G. Hall, J.B. Decoste, G.W. Peterson, R.Q. Snurr, C.J. Cramer, J.T. Hupp, O.F. Farha, Destruction of chemical warfare agents using metal-organic frameworks, Nat. Mater. 14 (2015) 512–516.
[30] P. Li, R.C. Klet, S.-Y. Moon, T.C. Wang, P. Deria, A.W. Peters, B.M. Klahr, H.-J. Park, S.S. Al-Juaid, J.T. Hupp, O.K. Farha, Synthesis of nanocrystals of Zr-based metal–organic frameworks with csq-net: significant enhancement in the degradation of a nerve agent simulant, Chem. Commun. 51 (2015) 10925–10928.
[31] S.Y. Moon, E. Proussaloglou, G.W. Peterson, J.B. DeCoste, M.G. Hall, A.J. Howarth, J.T. Hupp, O.K. Farha, Detoxification of chemical warfare agents using a Zr6-based metal–organic framework/polymer mixture, Chem. - A Eur. J. 22 (2016) 14864–14868.
[32] Y. Han, M. Liu, K. Li, Y. Zuo, Y. Wei, S. Xu, G. Zhang, C. Song, Z. Zhang, X. Guo, Facile synthesis of morphology and size-controlled zirconium metal–organic framework UiO-66: the role of hydrofluoric acid in crystallization, CrystEngComm 17 (2015) 6434–6440.
[33] M. Vandichel, J. Hajek, F. Vermoortele, M. Waroquier, D.E. De Vos, V. Van Speybroeck, Active site engineering in UiO-66 type metal–organic frameworks by intentional creation of defects: a theoretical rationalization, CrystEngComm 17 (2015) 395–406.
[34] Y. Zhao, D.G. Truhlar, A new local density functional for main-group thermochemistry, transition metal bonding, thermochemical kinetics, and noncovalent interactions, J. Chem. Phys. 125 (2006) 194101.
[35] F. Weigend, R. Ahlrichs, Balanced basis sets of split valence, triple zeta valence and quadruple zeta valence quality for H to Rn: design and assessment of accuracy, Phys. Chem. Chem. Phys. 7 (2005) 3297–3305.
[36] M. Dolg, W. Wedig, H. Stoll, H. Preuss, Energy-adjusted ab initio pseudopotentials for the first row transition elements, J. Chem. Phys. 86 (1986) 866–872.
[37] Y. Shao, et al., Advances in molecular quantum chemistry contained in the q-chem 4 program package, Mol. Phys. 113 (2015) 184–215.
[38] M.R. DeStefano, T. Islamoglu, S.J. Garibay, J.T. Hupp, O.K. Farha, Room-temperature synthesis of UiO-66 and thermal modulation of densities of defect sites, Chem. Mater. 29 (2017) 1357–1361.
[39] B.S.J. Garibay, S.M. Cohen, Isoreticular synthesis and modification of frameworks with the UiO-66 topology, Chem. Commun. 46 (2010) 7700.
[40] K.Y. Cho, Y.S. Yeom, H.Y. Seo, P. Kumar, A.S. Lee, K.-Y. Baek, H.G. Yoon, Ionic block copolymer doped reduced graphene oxide supports with ultra-fine Pd nanoparticles: strategic realization of ultra-accelerated nanocatalysis, J. Mater. Chem. A 3 (2015) 20471–20476.
[41] T.H. Kwon, K.Y. Cho, K.-Y. Baek, H.G. Yoon, B.M. Kim, Recyclable palladium–graphene nanocomposite catalysts containing ionic polymers: efficient Suzuki coupling reactions, RSC Adv. 7 (2017) 11684–11690.
[42] K.Y. Cho, H.Y. Seo, Y.S. Yeom, P. Kumar, A.S. Lee, K.Y. Baek, H.G. Yoon, Stable 2D-structured supports incorporating ionic block copolymer-wrapped carbon nanotubes with graphene oxide toward compact decoration of metal nanoparticles and

high-performance nano-catalysis, Carbon 105 (2016) 340–352.
[43] K.Y. Cho, H.-J. Kim, X.H. Do, J.Y. Seo, J.-W. Choi, S.-H. Lee, H.G. Yoon, S.S. Hwang, K.-Y. Baek, Synthesis of water soluble metalloporphyrin-cored amphiphilic star block copolymer photocatalysts for an environmental application, Res. Chem. Intermed. 44 (2018) 4663–4684.
[44] P. Hu, M. Long, Cobalt-catalyzed sulfate radical-based advanced oxidation: a review on heterogeneous catalysts and applications, Appl. Catal. B 181 (2016) 103–117.
[45] J. Pritchard, F.A. Filonenko, R. van Putten, E.J.M. Hensen, E.A. Pidko, Heterogeneous and homogeneous catalysis for the hydrogenation of carboxylic acid derivatives: history, advances and future directions, Chem. Soc. Rev. 44 (2015) 3808–3833.
[46] S.H. Lee, H.Y. Seo, Y.S. Yeom, J.E. Kim, H. An, J.-S. Lee, H.-K. Jeong, K.-Y. Baek, K.Y. Cho, H.G. Yoon, Rational design of epoxy/ ZIF-8 nanocomposites for enhanced suppression of copper ion migration, Polymer 150 (2018) 159–168.
[47] J. Kim, S.-N. Kim, H.-G. Jang, G. Seo, W.-S. Ahn, CO_2 cycloaddition of styrene oxide over MOF catalysts, Appl. Catal. A Gen. 453 (2013) 175–180.
[48] K.Y. Cho, Y.S. Yeom, H.Y. Seo, Y.H. Park, H.N. Jang, K.-Y. Baek, H.G. Yoon, Rational design of multiamphiphilic polymer compatibilizers: versatile solubility and hybridization of noncovalently functionalized CNT nanocomposites, ACS Appl. Mater. Interfaces 7 (2015) 9841–9850.
[49] R. Lakshmanan, M. Sanchez-Dominguez, J.A. Matutes-Aquino, S. Wennmalm, G. Kuttuva Rajarao, Removal of total organic carbon from sewage wastewater using poly(ethylenimine)-functionalized magnetic nanoparticles, Langmuir 30 (2014) 1036–1044.
[50] S.G. Ryu, M.K. Kim, M.G. Park, S.O. Jang, S.H. Kim, H.S. Jung, Availability of Zr-based MOFs for the degradation of nerve agents in all humidity conditions, Microporous Mesoporous Mater. 274 (2019) 9–16.
[51] T.W. Zerda, G. Hoang, Effect of solvents on the hydrolysis reaction of tetramethyl ort hosilicate, Chem. Mater. 2 (1990) 372–376.
[52] L. Hu, L. Lin, Z. Wu, S. Zhou, S. Liu, Chemocatalytic hydrolysis of cellulose into glucose over solid acid catalysts, Appl. Catal. B 174-175 (2015) 225–243.
[53] S.-S. Hsieh, J.J. Pignatello, Activated carbon-mediated base hydrolysis of alkyl bromides, Appl. Catal. B 211 (2017) 68–78.
[54] A. Veeken, B. Hamelers, Effect of temperature on hydrolysis rates of selected bio-waste components, Bioresour. Technol. 69 (1999) 249–254.